Free Energy Landscape of Type III Fibronectin Domain with Identified Intermediate State and Hierarchical Symmetry

Hao Sun,[1,2] Zilong Guo,[2] Haiyan Hong,[1] Zhuwei Zhang,[1,2] Yuhang Zhang,[1] Yang Wang,[2] Shimin Le,[1] and Hu Chen[1,2,*]
[1]Research Institute for Biomimetics and Soft Matter, Fujian Provincial Key Lab for Soft Functional Materials Research, Department of Physics, Xiamen University, Xiamen 361005, China
[2]Center of Biomedical Physics, Wenzhou Institute, University of Chinese Academy of Sciences, Wenzhou 325000, China

(Received 17 December 2022; accepted 23 October 2023; published 22 November 2023)

The tenth domain of type III fibronectin ($FNIII_{10}$) mediates cell adhesion to the extracellular matrix. Despite its structural similarity to immunoglobulin domains, $FNIII_{10}$ exhibits unique unfolding behaviors. We employed magnetic tweezers to investigate the unfolding and folding dynamics of $FNIII_{10}$ under physiological forces (4–50 pN). Our results showed that $FNIII_{10}$ follows a consistent transition pathway with an intermediate state characterized by detached A and G β strands. We determined the folding free energies and all force-dependent transition rates of $FNIII_{10}$ and found that both unfolding rates from the native state to the intermediate state and from the intermediate state to the unfolded state deviate from Bell's model. We constructed a quantitative free energy landscape with well-defined traps and barriers that exhibits a hierarchical symmetrical pattern. Our findings provide a comprehensive understanding of $FNIII_{10}$ conformational dynamics and demonstrate how free energy landscape of multistate biomolecules can be precisely mapped, illuminating the relationship between thermal stability, intermediate states, and folding rates in protein folding.

DOI: 10.1103/PhysRevLett.131.218402

Fibronectin (FN) is one of the crucial fibrous proteins in the extracellular matrix (ECM). Cell adhesion to ECM is mediated by the central cell-binding domain of FN, the tenth type III FN domain ($FNIII_{10}$), through the amino acid triplet Arg-Gly-Asp (RGD) which binds to the transmembrane receptor integrins [1]. The functions of FN are therefore essential for biological processes including cell growth, migration and differentiation [2–4], and oncogenic transformation [5–7]. There is increasing evidence indicating that the mechanical forces generated by the intracellular contractile machinery to FN have an important role in the regulation of FN fibrillogenesis and cell adhesion [8–10].

$FNIII_{10}$ has a characteristic immunoglobulin (Ig) β-sandwich native structure with seven β strands [11], However, its thermodynamic properties are dramatically different from typical Ig domains [12,13]. Bulk experiments, single-molecule force spectroscopy (SMFS) experiments [14], and computer simulations have been used to study the properties of FNIII modules. Measurements by scanning calorimetry and fluorescence spectroscopy demonstrate that $FNIII_{10}$ is one of the most thermostable FNIII modules [15,16]. On the other hand, SMFS experiments using atomic force microscope (AFM) have revealed $FNIII_{10}$ as one of the mechanically weakest FNIII modules [17,18]. Molecular dynamics (MD) simulations gave the unfolding pathways of $FNIII_{10}$ involving several major intermediate (I) states [19–22]. Further AFM experiments indicated that $FNIII_{10}$ unfolds in two possible pathways: an apparent two-state unfolding transition as well as a majority of unfolding pathways through two possible I states [23], and the protein-substrate interactions may affect the unfolding process [24].

Comprehensive understanding of these distinct properties of $FNIII_{10}$ is still missing and needs further study. Firstly, both simulations and AFM experiments were done at high force regime greater than 50 pN. The force response of $FNIII_{10}$ to lower forces, particularly in physiological conditions, has not been investigated. Furthermore, little effort has been put on detailed force-dependent kinetics measurements. As a result, the transition parameters between different states of $FNIII_{10}$ at physiological forces need to be accurately quantified.

Here we measured the response of $FNIII_{10}$ to mechanical forces of 4–50 pN by magnetic tweezers (MT). A clear intermediate state exists during the unfolding process of $FNIII_{10}$. From three different truncations of $FNIII_{10}$ as the candidates, we identified the unique intermediate state which has A and G β strands detached from the native structure of $FNIII_{10}$. The equilibrium folding and unfolding process of $FNIII_{10}$ is recorded for the first time to determine its folding free energy. All possible transition rates among the native (N) state, the I state, and the unfolded (U) state are determined as functions of stretching force. Furthermore, the free energy landscape of $FNIII_{10}$ with detailed knowledge of multiple traps and barriers is constructed.

Unfolding intermediate state identification.—In MT experiments, the protein construct of (biotin)-AviTag-$2\times$I27-$FNIII_{10}$-$2\times$I27-SpyTag is conjugated between

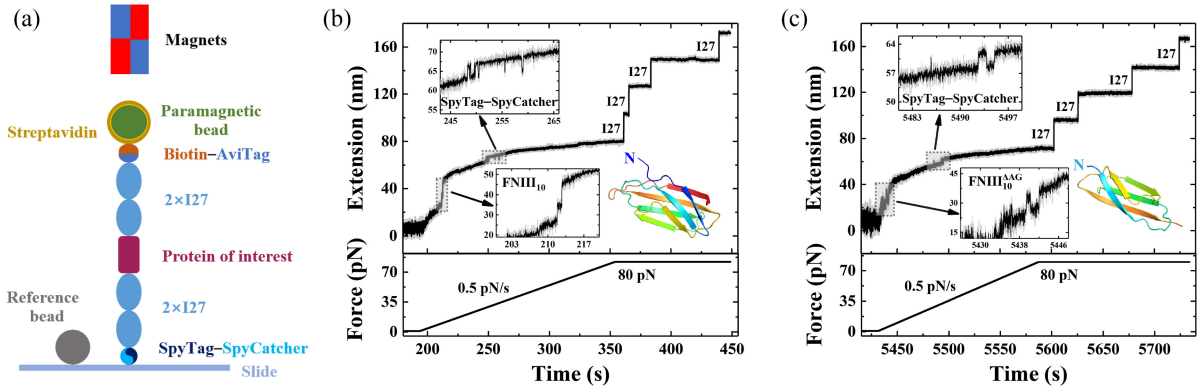

FIG. 1. Single-molecule force spectroscopy measurements with MT. (a) Schematic representation of protein construct in MT (not drawn in proportion). The reference bead is used to remove the drift. (b) $FNIII_{10}$ (amino acids (a.a.) 1–94, protein data bank:1ttf) and (c) $FNIII_{10}^{\Delta AG}$ (a.a. 13–80) unfolding, SpyTag–SpyCatcher (un)zipping, and I27 unfolding events were recorded sequentially when force increases from 1 to 80 pN with loading rate of 0.5 pN/s. Insets show the native structure of $FNIII_{10}$ (b) and $FNIII_{10}^{\Delta AG}$ (c). Raw data in (b) and (c) recorded at a sampling rate of 200 Hz (gray) are smoothed using 50-ms time window (black). Uncertainty of force is estimated as 5%.

SpyCatcher-modified cover slip and streptavidin-coated paramagnetic bead [Fig. 1(a)]. First of all, we carried out force-ramp experiments from 1 to 80 pN with loading rate of 0.5 pN/s. Single protein tether was confirmed by the fingerprint signals of SpyTag–SpyCatcher and $4 \times$ I27 [Fig. 1(b)] [25]. At about 10 pN, we observed unfolding transition of $FNIII_{10}$ with two consecutive steps, suggesting the presence of I state.

MD simulations of $FNIII_{10}$ indicate that the intermediate state has three candidates with AB, AG, or FG β strands peeled from the native structure, respectively [20,21]. To identify the intermediate state, we constructed three truncations of $FNIII_{10}$: $FNIII_{10}^{\Delta AB}$, $FNIII_{10}^{\Delta AG}$, and $FNIII_{10}^{\Delta FG}$, corresponding to the protein constructs with AB, AG, and FG β strands of $FNIII_{10}$ removed, respectively [Fig. S1(a) [26]].

We employed similar force-ramp experiments on the three truncations of $FNIII_{10}$. It was found that only $FNIII_{10}^{\Delta AG}$ exhibited a clear unfolding step on the extension time course [Fig. 1(c)]. In contrast, $FNIII_{10}^{\Delta AB}$ and $FNIII_{10}^{\Delta FG}$ did not show any additional unfolding steps except the fingerprint signals of SpyTag-SpyCatcher and $4 \times$ I27 [Figs. S1(b) and S1(c) [26]]. Besides this, we constructed a single domain of $FNIII_{10}$ and three truncations without $4 \times$ I27, AviTag, and SpyTag. The UV absorption spectra of the AKTA protein purification system suggests that only $FNIII_{10}$ and $FNIII_{10}^{\Delta AG}$ have stable compact structures [Fig. S1(d) [26]]. Differential scanning calorimetry measurement shows that the melting temperature of $FNIII_{10}^{\Delta AG}$ is approximately 10 K lower than $FNIII_{10}$, indicating that $FNIII_{10}^{\Delta AG}$ has a well-defined structure with lower stability than $FNIII_{10}$ [Fig. S1(e) [26]]. In force-ramp MT experiments, after $FNIII_{10}$ and $FNIII_{10}^{\Delta AG}$ were unfolded, clear folding steps were recorded during the force-decreasing process (Fig. S2 [26]). Therefore, $FNIII_{10}^{\Delta AG}$ is identified as the unfolding intermediate state of $FNIII_{10}$ observed in MT experiments. It is noteworthy that the I state of $FNIII_{10}$ can fold back to the N state at times during the force-increasing process [Fig. S2(a) [26]].

Apparent two-state transitions of $FNIII_{10}$ *at low forces.*—Taking advantage of the intrinsic constant force capability of MT, we measured the folding and unfolding transitions at different constant forces. The left one-quarter panel of Fig. 2(a) shows the typical folding process of $FNIII_{10}$ at forces smaller than 6.5 pN. Starting from the U state which is held at 12 pN, we drop the force to smaller values of 6 pN and record a one-step refolding transition of $FNIII_{10}$. The lifetime of the U state gives the folding rates k^{UN} in the force range of 4–6.5 pN [Fig. 2(c) herein and Fig. S3 in Ref. [26]].

When the protein is held by constant forces between 6.5 and 8 pN, we can observe multiple equilibrium folding and unfolding transitions of $FNIII_{10}$ in the timescale of about an hour [Fig. 2(b)]. From the lifetimes of U and N states, the folding rate k^{UN} and unfolding rate k^{NU} were determined [Fig. 2(c) herein and Fig. S4 in Ref. [26]]. Critical force with equal k^{UN} and k^{NU}, $F_c^{NU} = 7.4$ pN, which gives folding free energy of $16.9 k_B T$, where k_B denotes Boltzmann constant and T the absolute room temperature. Please note that we can hardly observe the I state in the folding and unfolding processes at forces below 8 pN, which might be due to its short lifetime in this force range.

Unfolding transition with I state at high forces.—The right three-fourths panel of Fig. 2(a) exhibits the representative unfolding process of $FNIII_{10}$. Firstly, $FNIII_{10}$ folded to the N state at 1 pN. Then force was increased abruptly to high forces (9, 15, and 40 pN). When the force is in the range of 8–12 pN, reversible transition N⇄I can be observed. Once the force is greater than 15 pN, the transition I → N cannot be observed, while irreversible transitions N → I, I → U, or apparent unfolding transition directly N → U can be recorded.

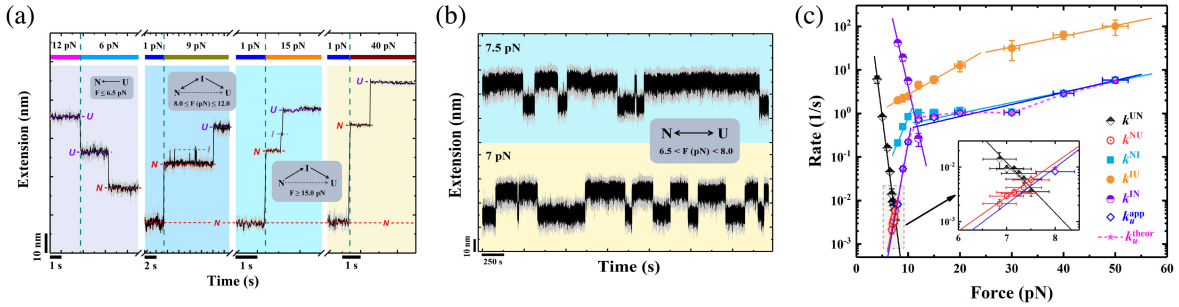

FIG. 2. Force-dependent folding and unfolding transitions of $FNIII_{10}$. (a) Typical folding and unfolding processes of $FNIII_{10}$ were recorded by MT. Specifically, one-step folding processes of $FNIII_{10}$ were observed when force dropped from 12 to 6 pN. Apparently, different unfolding pathways were observed when force jumps from 1 pN to 9, 15, and 40 pN. (b) At constant forces of 7 and 7.5 pN, extension traces show the equilibrium folding and unfolding transitions between N and U states of $FNIII_{10}$. Raw data in (a) and (b) with a sampling rate of 200 Hz (gray) are smoothed using 50-ms time window (black). (c) Average folding rates (k^{UN}) at forces smaller than 6.5 pN, equilibrium folding and unfolding rates (k^{UN} and k^{NU}) from 6.85 to 7.5 pN (enlarged figure), and transition rates (k^{NI}, k^{IN}, k^{IU}, and k_u^{app}) at forces greater than 8 pN of $FNIII_{10}$ are acquired from more than four independent tethers. $k^{NI}(F)$, $k^{IU}(F)$, and $k_u^{app}(F)$ show nonlinear behavior deviating from the prediction of Bell's model. Theoretical unfolding rate from N to U (k_u^{theor}) calculated from Eq. (2) agrees well with experimental k_u^{app}. The solid lines (the same color as corresponding symbols) are fitting results by Bell's model in different force ranges. Uncertainty of force is estimated as 5%.

In order to acquire all available transition rates among the N, I, and U states of $FNIII_{10}$ under constant forces, we repeated the force-jump experiments with multiple cycles to collect enough data for statistical analysis. The lifetimes (τ_N and τ_I) were obtained by exponential fitting of the survival probabilities of N and I states, respectively (Fig. S5 [26]). The transition rate from N to I (k^{NI}) is the reciprocal of τ_N, while the transition rates k^{IN} and k^{IU} can be obtained from τ_I and the counts ratio of transitions I → N and I → U (Fig. S6 [26]). In the entire measured force range, non-monotonic force-dependent τ_I with a peak value of 0.21 s at 12 pN is due to the opposite force dependence of k^{IN} and k^{IU} [Fig. S6(a) [26]].

All measured force-dependent transition rates among the N, I, and U states of $FNIII_{10}$ are shown in Fig. 2(c). The intersection of $k^{NI}(F)$ and $k^{IN}(F)$ determines the critical force $F_c^{NI} \sim 11.1$ pN, which gives the free energy difference between N and I states as $11.5k_BT$, which might come partially from the hydrogen bonds involving AG β strands (Table S1 of Ref. [26]). Considering the folding free energy of $16.9k_BT$ for $FNIII_{10}$, I state has folding free energy of $5.4k_BT$. The 10 K lower melting temperature for $FNIII_{10}^{\Delta AG}$ agrees with the smaller entropy cost to form I state than N state (Fig. S7 [26]).

We found that both unfolding rates $k^{NI}(F)$ and $k^{IU}(F)$ show nonlinear force dependence with different slopes at different force ranges. From 12 to 50 pN, fitting of $k^{NI}(F)$ using Bell's model $k(F) = k_0 \exp(Fx_u/k_BT)$ gives unfolding distance $x_{u,1}^{NI} = 0.23 \pm 0.04$ nm and zero-force unfolding rate $k_{0,1}^{NI} = 0.33\ s^{-1}$. While in the force range of 8–10 pN, the fitting yields $x_{u,2}^{NI} = 2.7 \pm 0.4$ nm, which is more than 10 times longer than $x_{u,1}^{NI}$, and $k_{0,2}^{NI} = 1.1 \times 10^{-3}\ s^{-1}$. In the force range 30–50 pN, fitting of $k^{IU}(F)$ gives $x_{u,1}^{IU} = 0.23 \pm 0.02$ nm, while fitting in 8–20 pN gives $x_{u,2}^{IU} = 0.65 \pm 0.05$ nm.

Unified unfolding pathway of $FNIII_{10}$ *through I state.*— Apparently $FNIII_{10}$ unfolds directly from N to U at low forces, and through I state at high forces. The connection of these two seemingly contrary unfolding pathways at different force ranges deserves further investigation.

To compare with results from equilibrium measurements, we neglect intentionally the I state to get an apparent unfolding rate (k_u^{app}) at force greater than 8 pN, which is the reciprocal of the apparent unfolding time (t_u^{app}) defined as the time spent from N to U (Fig. S8 [26]). The average force-dependent apparent unfolding rates obtained from both equilibrium measurements and force-jump experiments are summarized in Fig. 2(c). The unfolding rates of 6.85–7.5 pN obtained in equilibrium measurements are on the same line with the k_u^{app} of 8–10 pN acquired from the force-jump experiments, which indicates that unfolding of $FNIII_{10}$ is going through the same pathway with I state though it is not recorded directly due to its short lifetime at forces lower than 8 pN [Fig. S6(a) [26]]. Therefore, one single unfolding pathway is sufficient to describe the unfolding process over the entire experimental force range:

$$N \rightleftarrows I \rightarrow U. \tag{1}$$

The theoretical apparent unfolding rate (k_u^{theor}) from N to U is given by [27]

$$k_u^{theor}(F) = \frac{k^{NI}(F)k^{IU}(F)}{k^{NI}(F) + k^{IU}(F) + k^{IN}(F)}. \tag{2}$$

We can calculate k_u^{theor} on the basis of experimental data k^{NI}, k^{IU}, and k^{IN}. It is of no surprise that $k_u^{theor}(F)$ is in perfect agreement with $k_u^{app}(F)$ [Fig. 2(c)].

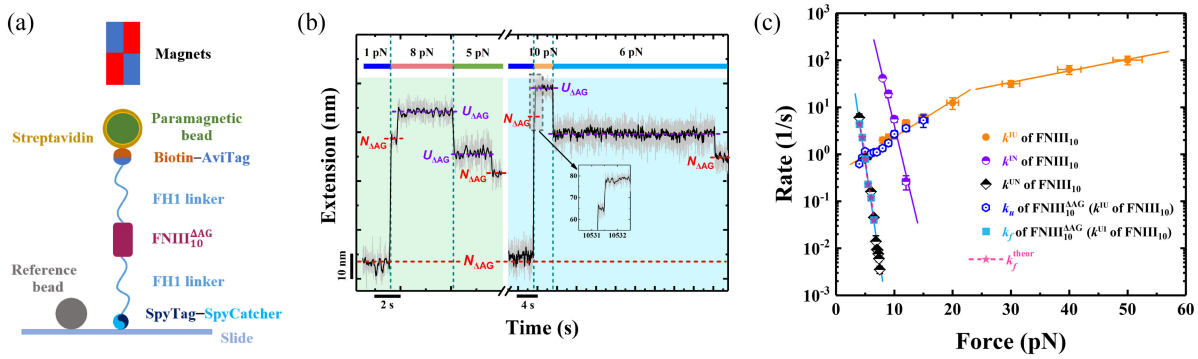

FIG. 3. Force-dependent folding and unfolding dynamics of $FNIII_{10}^{\Delta AG}$ and comparison with $FNIII_{10}$. (a) Schematic representation of protein construct of AviTag-FH1-$FNIII_{10}^{\Delta AG}$-FH1-SpyTag in MT. (b) Typical unfolding and folding processes of $FNIII_{10}^{\Delta AG}$ were recorded in force-jump experiments. High forces (8 and 10 pN) allow $FNIII_{10}^{\Delta AG}$ to unfold, and low forces (5 and 6 pN) ensure to observe folding transition of $FNIII_{10}^{\Delta AG}$. Raw data with a sampling rate of 200 Hz (gray) are smoothed using 250-ms time window (black). (c) Force-dependent folding and unfolding rates of $FNIII_{10}^{\Delta AG}$ were summarized from force-jump measurements. k_u of $FNIII_{10}^{\Delta AG}$ agrees with k^{IU} of $FNIII_{10}$ in the force range from 8 to 15 pN. k_f of $FNIII_{10}^{\Delta AG}$, $k^{UN}(F)$ of $FNIII_{10}$, and $k_f^{theor}(F)$ calculated from Eq. (3) are consistent with each other. The solid lines (the same color as the corresponding experimental data points) are the fitting results based on Bell's model in different force ranges. Uncertainty of force is estimated to be 5%.

Beyond that, we extracted the extension step sizes for the transitions $N \rightleftarrows I$ (NI) and $I \rightarrow U$ (IU) as well as for the apparently full transition $N \rightarrow U$ (NU^{app}) from multiple force-jump experiments (Fig. S9 [26]). The resulting force-step size curves are well described by the wormlike chain model [28] with a persistence length of 0.8 nm, yielding contour length difference of 11.2 ± 0.2 nm between N and I, 17.5 ± 0.2 nm between I and U, and 28.3 ± 0.3 nm between N and U, respectively, which are consistent with the number of unfolded amino acids.

Folding dynamics of $FNIII_{10}$ *revealed by* $FNIII_{10}^{\Delta AG}$.—As the reverse process of unfolding, folding of $FNIII_{10}$ should go through pathway $U \rightleftarrows I \rightarrow N$. But we cannot record the folding transition from U to I on wild-type $FNIII_{10}$. Given I state is $FNIII_{10}^{\Delta AG}$, we measured the folding and unfolding dynamics of $FNIII_{10}^{\Delta AG}$ using protein construct: (biotin)-AviTag-FH1-$FNIII_{10}^{\Delta AG}$-FH1-SpyTag, where FH1 is a flexible peptide linker with 35 residues from human formin Mdia1 [29,30] [Fig. 3(a)].

In a typical force-jump measurement, the force jumped from 1 pN to higher values of 8 and 10 pN at which clear unfolding steps of $FNIII_{10}^{\Delta AG}$ were recorded. Then force was dropped to 5 and 6 pN to allow folding of $FNIII_{10}^{\Delta AG}$ [Fig. 3(b)]. The folding rate at 4–6.5 pN and unfolding rate at 4–15 pN of $FNIII_{10}^{\Delta AG}$ were obtained [Fig. 3(c) herein and Fig. S10 [26]]. The consistent unfolding rates of $FNIII_{10}^{\Delta AG}$ and k^{IU} of $FNIII_{10}$ from 4 to 20 pN can be fitted by Bell's model with $x_{u,2}^{IU} = 0.73 \pm 0.03$ nm and $k_{0,2}^{IU} = 0.39\ s^{-1}$, which are refinement of previous fitting results.

Based on the intersection of force-dependent unfolding and folding rates of $FNIII_{10}^{\Delta AG}$ [Fig. 3(c)], the critical force of $FNIII_{10}^{\Delta AG}$ is about 4.8 pN, which gives zero-force folding free energy of $\sim 4.9 k_B T$ for $FNIII_{10}^{\Delta AG}$.

The theoretical apparent folding rate (k_f^{theor}) of $FNIII_{10}$ is given by [27]

$$k_f^{theor}(F) = \frac{k^{UI}(F) k^{IN}(F)}{k^{UI}(F) + k^{IN}(F) + k^{IU}(F)}. \quad (3)$$

The measured folding rate of $FNIII_{10}$ (k^{UN}) agrees perfectly with k_f^{theor} based on experimental data of k^{UI}, k^{IN}, and k^{IU} [Fig. 3(c)]. Please note that k^{IN} below 8 pN are acquired by extrapolation, k^{UI} and k^{IU} of $FNIII_{10}$ are obtained from the folding and unfolding rates of $FNIII_{10}^{\Delta AG}$, respectively. k^{UN} from $FNIII_{10}$ and k^{UI} from $FNIII_{10}^{\Delta AG}$ completely superimpose each other at forces below 6.5 pN. At this force range, k^{UI} is much smaller than k^{IN} by approximately 3 orders of magnitude. Therefore, the $U \rightarrow I$ transition is the rate-limiting step of the folding process of $FNIII_{10}$.

Furthermore, the step sizes of $FNIII_{10}^{\Delta AG}$ agree well with those of transition from I to U for $FNIII_{10}$ (Fig. S11 [26]). The consistent unfolding rates and step sizes for overlapping force ranges (8–15 pN) provide additional evidence to confirm that $FNIII_{10}^{\Delta AG}$ is the I state of $FNIII_{10}$.

Free energy landscape of $FNIII_{10}$.—The force responses over large force range offer the essential information to dissect the free energy landscape of $FNIII_{10}$. Based on the measured parameters of step size, critical force, and force-dependent unfolding and folding rates of $FNIII_{10}$ and $FNIII_{10}^{\Delta AG}$, we constructed a detailed free energy landscape of $FNIII_{10}$ along the reaction coordinate of extension with free energy of N state of $FNIII_{10}$ as the reference (Fig. 4).

Firstly, the distance between N and C termini of $FNIII_{10}$ is 3.14 nm in its native structure. From the critical force (7.4 pN) and step size ($\sim$16.3 nm) of transition between N and U of $FNIII_{10}$ in equilibrium measurements, U state has

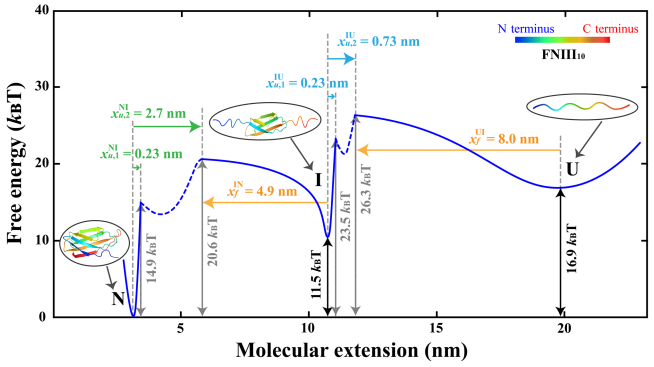

FIG. 4. The free energy landscape of $FNIII_{10}$ constructed by the information of the force sensitivity of the transition rates. Insets show the conformations of N, I, and U states of $FNIII_{10}$, respectively.

free energy of $16.9k_BT$ with extension of ~19.4 nm. Similarly, in terms of the critical force (11.1 pN) and step size (~7.6 nm) of transition between N and I of $FNIII_{10}$, I state has free energy of $11.5k_BT$ with extension of ~10.7 nm.

The information of transition barriers can be obtained from the fitting results of force-dependent transition rates k^{NI} and k^{IU}. Two distinct unfolding distances ($x_{u,1}^{NI} = 0.23$ nm and $x_{u,2}^{NI} = 2.7$ nm) were acquired by fitting $k^{NI}(F)$ of $FNIII_{10}$ in high-force and low-force regimes, which means that there are two energy barriers located at extension of about 3.4, and 5.8 nm, respectively. If we suppose the intrinsic transition rate (k^*) of $FNIII_{10}$ is $\sim 10^6$ s^{-1} [31], then the energy barriers ($\Delta G^{\ddagger}$) can be estimated as $14.9k_BT$ and $20.6k_BT$ according to an empirical equation: $k_0 = k^* \exp(-\Delta G^{\ddagger}/k_BT)$. Furthermore, the fitting of $k^{IN}(F)$ of $FNIII_{10}$ suggests that the folding distance from I state to N state (x_f^{IN}) of $FNIII_{10}$ is 4.9 nm, which gives consistent step size between N and I states at forces of 10–12 pN.

Similarly, the slopes of the two fitted lines for the unfolding rates of $FNIII_{10}^{\Delta AG}$ provide information of the two barriers between I and U of $FNIII_{10}$, which has unfolding distances $x_{u,1}^{IU} = 0.23$ nm and $x_{u,2}^{IU} = 0.73$ nm, respectively. These correspond to two energy barriers of $23.5k_BT$ and $26.3k_BT$ at extension of 10.9 and 11.4 nm, respectively. The folding distance (x_f^{UI}) obtained by fitting the folding rates of $FNIII_{10}^{\Delta AG}$ is 8.0 nm. $x_{u,2}^{IU} + x_f^{UI} \sim 8.7$ nm is consistent with the step size between I and U states at ~5 pN.

As the intermediate state of $FNIII_{10}$ is just the native state of $FNIII_{10}^{\Delta AG}$, the two free energy barriers between I and U states is not surprising. Intriguingly, only two β strands of $FNIII_{10}$ are peeled off during the transition process from N to I, but there are also two barriers between them. The extension difference between these two barriers is about 2.5 nm, which is approximately the extension of one β strand (A or G). Therefore, the obtained two barriers might come from the peeling transition of each β strand sequentially. This scenario is in agreement with previous coarse-grained and all-atomic MD simulations [21,32].

In summary, we examined the response of $FNIII_{10}$ to stretching forces applied between its N and C termini over physiological force range from 4 to 50 pN using MT. In the unfolding process of $FNIII_{10}$, there is a noticeable I state which is identified as $FNIII_{10}^{\Delta AG}$ from not only the step size, but also the thermal stability and force-dependent transition rates. Similar to some two-state proteins [33–35], overall the unfolding rates of $FNIII_{10}$ are more sensitive to low forces than high forces, which indicates that there is more than one barrier along the transition pathway. From the nonlinear force-dependent transition rates between N and I, and between I and U, quantitative free energy landscape along extension coordinate is constructed. The free energy landscape of $FNIII_{10}$ shows hierarchical symmetric feature with two barriers between N and I, and between I and U. From a physical perspective, force and extension are conjugate variables. Consequently, only low-force measurements can provide information on the free energy landscape across a broad range of extensions.

Fibronectin, as a main component of ECM, is subject to fluctuating external forces. Its stability and fast-folding property are crucial to maintain its biological function. The distinct dynamic properties of $FNIII_{10}$ compared to its structurally homologous Ig domains warrant further analysis. $FNIII_{10}$ has a folding free energy of $16.9k_BT$, twice the value for I27 ($8.3k_BT$; see Table S2 [26]) [13]. The substantial folding free energy of $FNIII_{10}$ allows for the presence of a stable partially folded intermediate state $FNIII_{10}^{\Delta AG}$. Though $FNIII_{10}^{\Delta AG}$ is not very stable, its stability is enough to function as the folding core of $FNIII_{10}$, upon which the reunification of A and G β strands enhances the stability of $FNIII_{10}$. In contrast, a similar truncation of I27 is expected to have higher free energy than the fully unfolded state, rendering it unable to assume an intermediate state (Fig. S12 [26]). The folding process of $FNIII_{10}$ is consistent with the nucleation-growth mechanism [36]. The transition of $FNIII_{10}$ from U to I can be interpreted as the nucleation process followed by a faster transition from I to N, ensuring a rapid folding rate of $FNIII_{10}$ which is 3 orders of magnitude higher than I27 at 5 pN (Table S2 [26]) due to the small size of $FNIII_{10}^{\Delta AG}$ [37]. Therefore, the characteristics of $FNIII_{10}$ not only provide profound insight into the interplay among stability, intermediate state, and folding rate in protein folding problems, but also suggest an efficient protein design strategy which modifies a folding core with additional stability-enhancing attachment to satisfy both stability and fast-folding requirements [38].

This work was supported by the National Natural Science Foundation of China (11874309 and 12174322), 111 project (B16029), and Research Fund of Wenzhou Institute (WIUCASQD2021008 and WIUCASQD2021043).

*chenhu@xmu.edu.cn

[1] J. C. Friedland, M. H. Lee, and D. Boettiger, Mechanically activated integrin switch controls $\alpha_5\beta_1$ function, Science **323**, 642 (2009).

[2] J. K. VanSlyke, B. A. Boswell, and L. S. Musil, Fibronectin regulates growth factor signaling and cell differentiation in primary lens cells, J. Cell Sci. **131** (2018).

[3] S. SenGupta, C. A. Parent, and J. E. Bear, The principles of directed cell migration, Nat. Rev. Mol. Cell Biol. **22**, 529 (2021).

[4] J. Patten and K. Wang, Fibronectin in development and wound healing, Adv. Drug Delivery Rev. **170**, 353 (2021).

[5] L. C. Plantefaber and R. O. Hynes, Changes in integrin receptors on oncogenically transformed cells, Cell **56**, 281 (1989).

[6] C. M. Williams, A. J. Engler, R. D. Slone, L. L. Galante, and J. E. Schwarzbauer, Fibronectin expression modulates mammary epithelial cell proliferation during acinar differentiation, Cancer Res. **68**, 3185 (2008).

[7] L. R. Wasil and K. H. Y. Shair, Epstein–Barr virus LMP1 induces focal adhesions and epithelial cell migration through effects on integrin-α_5 and N-cadherin, Oncogenesis **4**, e171 (2015).

[8] F. Kong, Z. Li, W. M. Parks, D. W. Dumbauld, A. J. a, A. P. Mould, M. J. Humphries, and C. Zhu, Cyclic mechanical reinforcement of integrin-ligand interactions, Mol. Cell **49**, 1060 (2013).

[9] N. Strohmeyer, M. Bharadwaj, M. Costell, R. Fässler, and D. J. Müller, Fibronectin-bound $\alpha_5\beta_1$ integrins sense load and signal to reinforce adhesion in less than a second, Nat. Mater. **16**, 1262 (2017).

[10] S. J. Tan, A. C. Chang, S. M. Anderson, C. M. Miller, L. S. Prahl, D. J. Odde, and A. R. Dunn, Regulation and dynamics of force transmission at individual cell-matrix adhesion bonds, Sci. Adv. **6**, eaax0317 (2020).

[11] A. L. Main, T. S. Harvey, M. Baron, J. Boyd, and I. D. Campbell, The three-dimensional structure of the tenth type III module of fibronectin: an insight into RGD-mediated interactions, Cell **71**, 671 (1992).

[12] M. Carrion-Vazquez, A. F. Oberhauser, S. B. Fowler, P. E. Marszalek, S. E. Broedel, J. Clarke, and J. M. Fernandez, Mechanical and chemical unfolding of a single protein: A comparison, Proc. Natl. Acad. Sci. U.S.A. **96**, 3694 (1999).

[13] H. Chen, G. Yuan, R. S. Winardhi, M. Yao, I. Popa, J. M. Fernandez, and J. Yan, Dynamics of equilibrium folding and unfolding transitions of titin immunoglobulin domain under constant forces, J. Am. Chem. Soc. **137**, 3540 (2015).

[14] M. Rief, M. Gautel, A. Schemmel, and H. E. Gaub, The mechanical stability of immunoglobulin and fibronectin III domains in the muscle protein titin measured by atomic force microscopy, Biophys. J. **75**, 3008 (1998).

[15] S. V. Litvinovich and K. C. Ingham, Interactions between type III domains in the 110 kD a cell-binding fragment of fibronectin, J. Mol. Biol. **248**, 611 (1995).

[16] E. Cota and J. Clarke, Folding of beta-sandwich proteins: three-state transition of a fibronectin type III module, Protein Sci. **9**, 112 (2000).

[17] A. F. Oberhauser, C. Badilla-Fernandez, M. Carrion-Vazquez, and J. M. Fernandez, The mechanical hierarchies of fibronectin observed with single-molecule AFM, J. Mol. Biol. **319**, 433 (2002).

[18] D. Craig, M. Gao, K. Schulten, and V. Vogel, Tuning the mechanical stability of fibronectin type III modules through sequence variations, Structure **12**, 21 (2004).

[19] E. Paci and M. Karplus, Forced unfolding of fibronectin type 3 modules: an analysis by biased molecular dynamics simulations, J. Mol. Biol. **288**, 441 (1999).

[20] M. Gao, D. Craig, V. Vogel, and K. Schulten, Identifying unfolding intermediates of FNIII(10) by steered molecular dynamics, J. Mol. Biol. **323**, 939 (2002).

[21] S. Mitternacht, S. Luccioli, A. Torcini, A. Imparato, and A. Irbäck, Changing the mechanical unfolding pathway of FnIII10 by tuning the pulling strength, Biophys. J. **96**, 429 (2009).

[22] M. Caraglio, A. Imparato, and A. Pelizzola, Pathways of mechanical unfolding of FnIII(10): Low force intermediates, J. Chem. Phys. **133**, 065101 (2010).

[23] L. Li, H. H. Huang, C. L. Badilla, and J. M. Fernandez, Mechanical unfolding intermediates observed by single-molecule force spectroscopy in a fibronectin type III module, J. Mol. Biol. **345**, 817 (2005).

[24] L. Donlon, D. Nordin, and D. Frankel, Complete unfolding of fibronectin reveals surface interactions, Soft Matter **8**, 9933 (2012).

[25] Z. Guo, H. Hong, H. Sun, X. Zhang, C. X. Wu, B. Li, Y. Cao, and H. Chen, SpyTag/SpyCatcher tether as a fingerprint and force marker in single-molecule force spectroscopy experiments, Nanoscale **13**, 11262 (2021).

[26] See Supplemental Material at http://link.aps.org/supplemental/10.1103/PhysRevLett.131.218402 for Supplementary Tables S1–S2 and Figs. S1–S12.

[27] C. A. Pierse and O. K. Dudko, Distinguishing signatures of multipathway conformational transitions, Phys. Rev. Lett. **118**, 088101 (2017).

[28] J. F. Marko and E. D. Siggia, Stretching DNA, Macromolecules **28**, 8759 (1995).

[29] D. R. Kovar, Molecular details of formin-mediated actin assembly, Curr. Opin. Cell Biol. **18**, 11 (2006).

[30] S. Le, X. Hu, M. Yao, H. Chen, M. Yu, X. Xu, N. Nakazawa, F. M. Margadant, M. P. Sheetz, and J. Yan, Mechanotransmission and mechanosensing of human alpha-actinin 1, Cell Rep. **21**, 2714 (2017).

[31] R. B. Best and G. Hummer, Diffusive model of protein folding dynamics with Kramers turnover in rate, Phys. Rev. Lett. **96**, 228104 (2006).

[32] D. K. Klimov and D. Thirumalai, Native topology determines force-induced unfolding pathways in globular proteins, Proc. Natl. Acad. Sci. U.S.A. **97**, 7254 (2000).

[33] Z. Guo, H. Hong, G. Yuan, H. Qian, B. Li, Y. Cao, W. Wang, C. X. Wu, and H. Chen, Hidden intermediate state and second pathway determining folding and unfolding dynamics of GB1 protein at low forces, Phys. Rev. Lett. **125**, 198101 (2020).

[34] H. Hong, Z. Guo, H. Sun, P. Yu, H. Su, X. Ma, and H. Chen, Free energy landscape with two barriers and a transient intermediate state determining the unfolding and folding dynamics of cold shock protein, Commun. Chem. **4**, 156 (2021).

[35] X. Ma, H. Sun, H. Hong, Z. Guo, H. Su, and H. Chen, Free-energy landscape of two-state protein acylphosphatase with large contact order revealed by force-dependent folding and unfolding dynamics, Phys. Rev. E **106**, 024404 (2022).

[36] E. D. Nelson and N. V. Grishin, Alternate pathways for folding in the flavodoxin fold family revealed by a nucleation-growth model, J. Mol. Biol. **358**, 646 (2006).

[37] A. N. Naganathan and V. Muñoz, Scaling of folding times with protein size, J. Am. Chem. Soc. **127**, 480 (2005).

[38] D. Baker, What has de novo protein design taught us about protein folding and biophysics? Protein Sci. **28**, 678 (2019).